Thermochimica Acta 579 (2014) 86–92

Contents lists available at ScienceDirect

Thermochimica Acta

journal homepage: www.elsevier.com/locate/tca

# Preparation and characterization of melt intercalated poly(ethylene oxide)/lithium montmorillonite nanocomposites

M. Erceg[a,*], D. Jozić[b], I. Banovac[a], S. Perinović[a], S. Bernstorff[c]

[a] Department of Organic Technology, Faculty of Chemistry and Technology, University of Split, Teslina 10/V, 21000 Split, Croatia
[b] Department of Inorganic Technology, Faculty of Chemistry and Technology, University of Split, Teslina 10/V, 21000 Split, Croatia
[c] Elettra-Sincrotrone Trieste S.C.p.A., Strada Statale 14, km 163.5 in AREA Science Park, 34149 Basovizza, Trieste, Italy

ARTICLE INFO

*Article history:*
Received 14 October 2013
Received in revised form 24 January 2014
Accepted 27 January 2014
Available online 8 February 2014

*Keywords:*
Poly(ethylene oxide)
Nanocomposites
Crystallinity
Thermal degradation
Kinetic analysis

ABSTRACT

The structure, crystallinity, thermal properties, kinetic analysis of thermal degradation and ionic conductivity of poly(ethylene oxide)/lithium montmorillonite (PEO/LiMMT) nanocomposites prepared by melt intercalation were investigated. An intercalated structure of PEO/LiMMT nanocomposites was found by small angle X-ray scattering (SAXS). Differential scanning calorimetry (DSC) shows that an addition of LiMMT decreases the crystallinity of PEO which completely disappears above 80 wt.% of LiMMT and decreases PEO melting temperature. The influence of LiMMT on the PEO crystallinity was also observed by SAXS and Fourier Transform Infrared Spectroscopy (FTIR). Thermogravimetric analysis (TGA) indicates that LiMMT significantly lowers the thermal stability of PEO and changes its degradation mechanism what is confirmed by kinetic analysis using isoconversional method and deconvolution procedure. Electrochemical impedance spectroscopy reveals the significant increase in ionic conductivity at room temperature with addition of LiMMT and optimum LiMMT content concerning conductivity was defined.



## 1. Introduction

Lithium ion secondary batteries are currently the best portable energy storage device for the consumer electronics market [1]. However, due to the usage of liquid organic solvents as electrolytes safety and ecological issues arise and manufacturers are turning to technology where liquid electrolyte is replaced with solid polymer electrolyte (SPE), i.e. to lithium polymer batteries. Lithium polymer batteries can be up to 20% lighter than lithium ion ones, they are much more flexible and can be as thin as a credit card. But, they are more expensive, lose capacity faster and the efficiency of their recycling is not satisfactory. Using biodegradable polymers, like poly(ethylene oxide) (PEO) as SPE can be advantageous from the ecological point of view. PEO based SPEs are among the most studied polymer ionic conductors [1–9]. Since ionic conductivity primarily takes place in the amorphous phase, the high crystallinity of PEO limits the lithium ion transport resulting in a poor ionic conductivity of PEO based electrolytes at room temperatures. Useful conductivity can be reached at temperatures above PEO melting point [10]. Some investigators tried to reduce PEO melting point by adding plasticizers, but this approach leads to a deterioration of the mechanical properties of PEO [11]. Incorporation of nanoclays in the PEO matrix may reduce the crystallinity of PEO and thus increase its ionic conductivity. This investigation is focused on the preparation and characterization of PEO nanocomposites with lithium montmorillonite (LiMMT) as nanoclay in order to establish the influence of LiMMT on the structure, crystallinity, thermal stability, thermal degradation mechanism of PEO as well as on its ionic conductivity.

## 2. Experimental part

### 2.1. Sample preparation

PEO powder with viscometric average molecular weight of 300,000 was purchased from Sigma–Aldrich. LiMMT was prepared by ion-exchange from natural montmorillonite (Cloisite®$Na^+$, Southern Clay Products Inc., USA) and lithium chloride (Kemika, Croatia). Ion-exchange has been carried out by suspending 15.0 g of Cloisite®$Na^+$ in 400 $cm^3$ of 1.0 mol/$dm^3$ LiCl solution in de-ionized water. The suspension was stirred with a magnetic stirrer for 48 h at 40 °C. The mixture was then centrifuged at 5000 rpm until a clear separation was obtained and the supernatant was decanted. A series of washings with de-ionized water and again centrifugation were performed until the chloride ions were completely removed (tested using $AgNO_3$ solution). The obtained residue is LiMMT.

* Corresponding author. Tel.: +385 21 329 459; fax: +385 21 329 461.
*E-mail address:* merceg@ktf-split.hr (M. Erceg).

0040-6031/$ – see front matter © 2014 Elsevier B.V. All rights reserved.
http://dx.doi.org/10.1016/j.tca.2014.01.024

LiMMT was then dried in an oven for 5 h at 120 °C and then in a vacuum oven for 48 h at 100 °C. PEO/LiMMT nanocomposites with compositions 90/10, 80/20, 70/30, 60/40, 50/50, 40/60, 30/70, 20/80 and 10/90 by weight were prepared by melt intercalation. Powders of PEO and LiMMT in the required weight ratios were manually mixed for 10 min using an agate mortar and shaped into pellets using a load of 5 tons produced by a hydraulic press. The obtained samples were 13 mm in diameter, with a thickness of 0.7–0.8 mm. Melt intercalation was performed at 90 °C for 8 h in a vacuum oven.

### 2.2. Testing methods

#### 2.2.1. Small angle X-ray scattering

Small angle X-ray scattering (SAXS) measurements were performed at the Austrian SAXS beamline at Elettra Sincrotrone Trieste S.C.p.A. The sample to detector distance was 1132 mm and photon energy of 8 keV was used (wavelength of 1.54 Å). Thus the $q$ value range was 0.09–7.58 $nm^{-1}$, which corresponds to a $d$ range 70.00–0.83 nm. The SAXS data have been collected by a MAR300 (MarResearch) Image plate, with exposition times of 1–2 s. The $q$ range of the scattering setup was calibrated using the AgBeh standard and all SAXS data were corrected for dark current and background. Lorentz correction was applied on the normalized data.

#### 2.2.2. Differential scanning calorimetry

Differential scanning calorimetry (DSC) measurements were performed with a Mettler-Toledo 823$^e$ calorimeter in nitrogen atmosphere (30 $cm^3$/min). The apparatus was calibrated with an indium standard. Samples of 11.8 ± 1.5 mg, encapsulated in aluminum pans, were firstly cooled to −90 °C. Then they were heated to 120 °C (heating rate of 20 °C/min – heating scan), kept there for 5 min and then cooled again to −90 °C (cooling rate of 20 °C/min – cooling scan). DSC measurements were performed according to ISO 11357-2 and ISO 11357-3 standards.

#### 2.2.3. Infrared spectroscopy

Infrared spectroscopy was performed with a Perkin-Elmer Spectrum One FT-IR spectrometer. FT-IR spectrograms (average of 40 scans) were recorded using the Horizontal Attenuated Total Reflectance (HATR) technique, with a ZnSe 45° crystal in the wave number range between 650 and 4000 $cm^{-1}$ and with a spectral resolution of 4 $cm^{-1}$. The samples were analysed in the form obtained after melt intercalation.

#### 2.2.4. Non-isothermal thermogravimetry

The thermal degradation (sample mass 9.3 ± 0.5 mg) was performed by the non-isothermal thermogravimetry (TGA) in the temperature range 50–500 °C at the heating rates 2.5, 5, 10 and 20 °C/min using a Perkin-Elmer Pyris 1 TGA. The nitrogen flow rate was 30 $cm^3$/min.

#### 2.2.5. Electrochemical impedance spectroscopy

Electrochemical impedance spectroscopy (EIS) was used for determination of the ionic conductivity of PEO/LiMMT nancomposites. The measurements were performed at 25 °C in the frequency range from 1 MHz to 1 Hz with the a.c. amplitude ± 20 mV using Solartron frequency response analyser 1255 and Solartron electrochemical interface 1287 controlled by PC. The experimental data were analysed using software Zview. PEO/LiMMT nanocomposites were sandwiched between two stainless steel (SS) blocking electrodes to form symmetrical SS/electrolyte/SS cell.

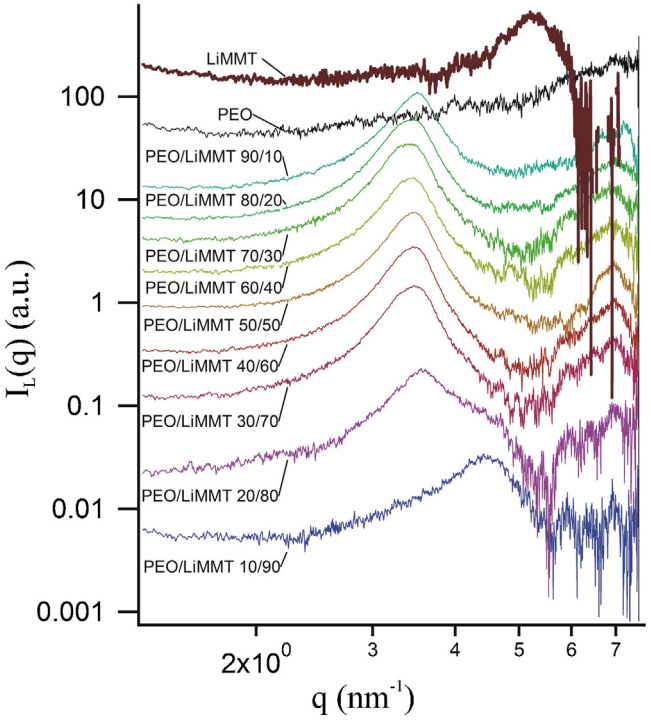


**Fig. 1.** SAXS patterns for PEO, LiMMT and PEO/LiMMT nanocomposites.

## 3. Results and discussion

### 3.1. Small angle X-ray scattering

The Lorentz-corrected SAXS profiles of PEO/LiMMT nanocomposites, pure LiMMT and PEO are shown in Fig. 1.

Pure LiMMT consists of alumina silicate layers stacked along a line perpendicular to the (0 0 1) basal plane where interlayers of pure LiMMT contain two planes of water molecules. The negative charge of the alumosilicate layers is compensated with exchangeable cations ($Li^+$) located in the interlayer gallery. The scattering peak of the pure LiMMT at the position $q$ = 5.21 $nm^{-1}$ corresponds to the interlayer distance of 1.20 nm (12.0 Å) ($d_{001}$). For pure PEO, the scattering peak which corresponds to the interlayer distance of 0.88 nm (8.8 Å) appears at $q$ = 7.15 $nm^{-1}$. The intercalation of polymers into layered inorganic compounds is generally unfavorable due to the high activation energy associated with the deformation of the crystal structure of the inorganic host. Thus, the intercalation requires the expansion of the interlayer spacing of layered compound. SAXS results show that PEO increases the interlayer distance of LiMMT (Fig. 2a).

In the sample with 10 wt.% of PEO the interlayer distance of LiMMT increases to 1.47 nm (14.7 Å) what is 22.5% expansion compared to pure LiMMT. Samples with higher amounts of PEO show higher but mutually similar values of LiMMT interlayer distances. The maximum value of 1.88 nm (18.8 Å) is observed for PEO/LiMMT 70/30 sample, where the increase amounts 56.7% of LiMMT original value. The scattering peak of LiMMT is present in the scattering curves of all samples, what suggests that exfoliation does not occur. The shift of the LiMMT scattering peak is a consequence of the PEO intercalation into its gallery. Intercalated PEO can be either in helical conformation or in a zigzag conformation what can be further analysed by infrared spectroscopy.

At the same time, the interlayer distance of PEO in nanocomposites increases by the addition of LiMMT up to a maximum value of 0.93 nm (9.3 Å) for nanocomposite assigned as PEO/LiMMT 70/30 (Fig. 2b). This suggests the conformational differences

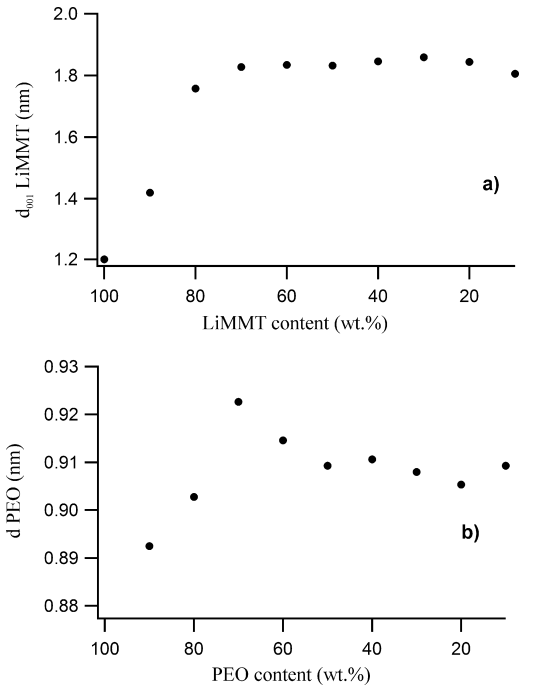


**Fig. 2.** *d*-Spacings for pure LiMMT (a) and PEO (b) and their sizes in PEO/LiMMT nanocomposites.

between pure and intercalated PEO that can cause changes of PEO crystallinity. In conclusion, the preparation of PEO/LiMMT nanocomposites is determined by the intercalation of PEO into the structure of LiMMT and with effect on the structure of PEO chains.

### 3.2. Differential scanning calorimetry

Normalized DSC heating curves of all samples are shown in Fig. 3. Characteristic melting temperatures (the extrapolated onset ($T_{eim}$) and end ($T_{efm}$) temperatures, the peak temperatures ($T_{pm}$)) as well as the melting enthalpies ($\Delta H_m$) were determined from DSC heating scans and given in Table 1.

Fig. 3 shows that samples up to 70 wt.% of LiMMT have one endothermic peak which represents melting of the crystalline phase in PEO. At LiMMT loadings higher than 70 wt.% melting peaks of PEO practically cannot be observed indicating that in those samples crystalline phase of PEO practically does not exist. $T_{eim}$, $T_{pm}$ and $T_{efm}$ values are lower in all PEO/LiMMT nanocomposites (where observable) compared to pure PEO (Table 1). Generally, lower melting temperatures of PEO in PEO/LiMMT nanocomposites can be ascribed to a disruption of its large scale crystalline formation by the presence of LiMMT. A similar behaviour for PEO nanocomposites has been observed before [5,6,12].

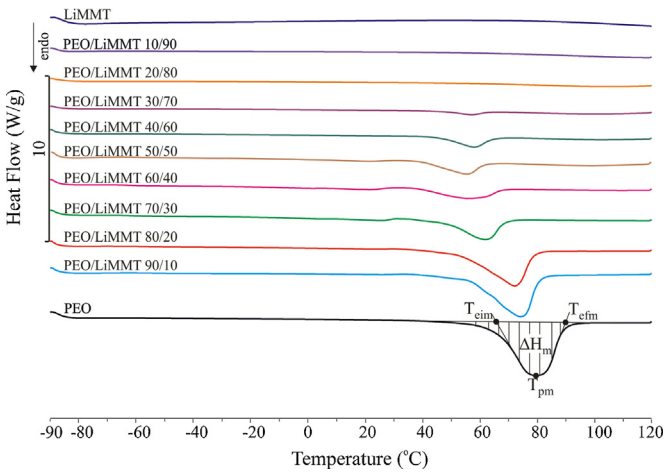


**Fig. 3.** Normalized DSC heating curves of all analysed samples.

$\Delta H_m$ values exhibit a continuous decrease with an increase of the LiMMT content in the nanocomposites (Fig. 3, Table 1). The question is whether this decrease is linear, i.e. is it due only to the lower amounts of PEO in samples. Namely, if LiMMT does not influence crystallinity of PEO at all, theoretical $\Delta H_{m,t}$ values proportional to the amount of PEO in samples should be obtained (Table 1). Since measured $\Delta H_m$ values are much lower than theoretical $\Delta H_{m,t}$ ones, obviously LiMMT influences PEO crystallinity. The proportion of the PEO crystalline phase, i.e. the degree of crystallinity $X_c$ is directly proportional to $\Delta H_m$ and is calculated according to Eq. (1) where $\Delta H_0$ is the melting enthalpy per unit weight of 100% crystalline PEO, which is 205 J/g [13] and $w$ is the weight fraction of PEO in the sample.

$$X_c = \frac{\Delta H_m}{\Delta H_0 \cdot w} \times 100 \quad (1)$$

As can be seen from Table 1, $X_c$ decreases with increasing clay content up to 80 wt.% of LiMMT when it completely disappears, although even at 70 wt.% of LiMMT $X_c$ is practically negligible. This phenomenon can be attributed to a steric hinderance of the PEO crystallization caused by the huge surface area of the clay and to the presence of $Li^+$. It is known from work on polymer electrolytes that the presence of small cationic species has an inhibiting effect on the crystallization of PEO as the polymer chain coordinates the cation which usually lowers the overall degree of crystallization [6,12].

The influence of LiMMT on the crystallization behaviour of PEO is also visible in DSC cooling scans shown in Fig. 4. The extrapolated onset ($T_{eic}$) and endset ($T_{efc}$) crystallization temperatures, the peak crystallization temperature ($T_{pc}$) as well as enthalpies of crystallization ($\Delta H_c$) were determined and their values given

**Table 1**
DSC data for PEO and PEO/LiMMT nanocomposites.

| Value | PEO/LiMMT | | | | | | | | | |
|---|---|---|---|---|---|---|---|---|---|---|
| | 100/0 | 90/10 | 80/20 | 70/30 | 60/40 | 50/50 | 40/60 | 30/70 | 20/80 | 10/90 |
| $T_{eim}$ (°C) | 60 | 57 | 52 | 47 | 39 | 38 | 46 | 48 | 50 | – |
| $T_{pm}$ (°C) | 75 | 73 | 71 | 61 | 56 | 47 | 57 | 57 | 52 | – |
| $T_{efm}$ (°C) | 87 | 80 | 78 | 68 | 68 | 56 | 64 | 63 | 54 | – |
| $-\Delta H_m$ (J/g) | 156.1 | 122.5 | 106.8 | 53.3 | 33.1 | 13.1 | 20.5 | 5.4 | 0.06 | – |
| $-\Delta H_{m,t}$ (J/g) | 156.1 | 140.5 | 124.9 | 109.3 | 93.7 | 78.1 | 62.4 | 46.8 | 31.2 | 15.6 |
| $X_c$ (%) | 76.1 | 66.4 | 64.7 | 37.1 | 26.9 | 12.8 | 25.0 | 8.8 | 0.2 | – |
| $T_{eic}$ (°C) | 41 | 41 | 42 | 35 | 38 | 22 | 28 | 32 | – | – |
| $T_{pc}$ (°C) | 35 | 35 | 37 | 29 | 30 | 15 | 22 | 22 | – | – |
| $T_{efc}$ (°C) | 26 | 28 | 28 | 16 | 7 | 5 | 4 | 10 | – | – |
| $\Delta H_c$ (J/g) | 127.8 | 104.1 | 91.2 | 49.6 | 27.1 | 18.8 | 16.8 | 2.9 | – | – |

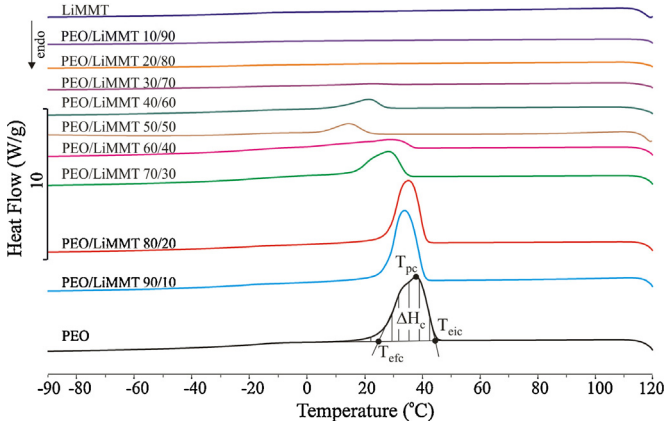


**Fig. 4.** Normalized DSC cooling curves of all analysed samples.

in Table 1. In nanocomposites up to 20 wt.% of LiMMT PEO displays crystallization temperatures similar to pure PEO while at higher LiMMT loadings the crystallization temperatures are shifted to lower temperatures. This means that at higher loadings crystallization is delayed by the addition of LiMMT, probably due to the higher undercooling needed to initiate crystallization. A similar behaviour for PEO nanocomposites has been observed before [5,6,12].

These results indicate that addition of LiMMT has an inhibiting effect on the crystallization and crystallinity degree of PEO. At LiMMT loadings higher than 70 wt.% crystallinity of PEO is practically negligible.

### 3.3. Infrared spectroscopy

FT-IR spectroscopy is a powerful tool for providing information regarding the difference between polymer and polymer/clay nanocomposites. FT-IR spectra of all samples are shown in Fig. 5.

The most significant changes are observed in the wave number region 3000–2750 $cm^{-1}$ and 1700–800 $cm^{-1}$. Pure PEO shows large broad band of asymmetric $-CH_2$ stretching between 3000 and 2750 $cm^{-1}$ while in nanocomposites this band broadens and splits at higher amounts of LiMMT. In the region between 1800 and 1700 $cm^{-1}$ new peaks appear in nanocomposites which cannot be observed nor in pure PEO neither in pure LiMMT. In the region between 1500 and 1200 $cm^{-1}$ peaks are getting broader and weaker compared to pure PEO. The peaks near 840 $cm^{-1}$ (designated with I. in Fig. 5) and 945 $cm^{-1}$ (designated with II. in Fig. 5)

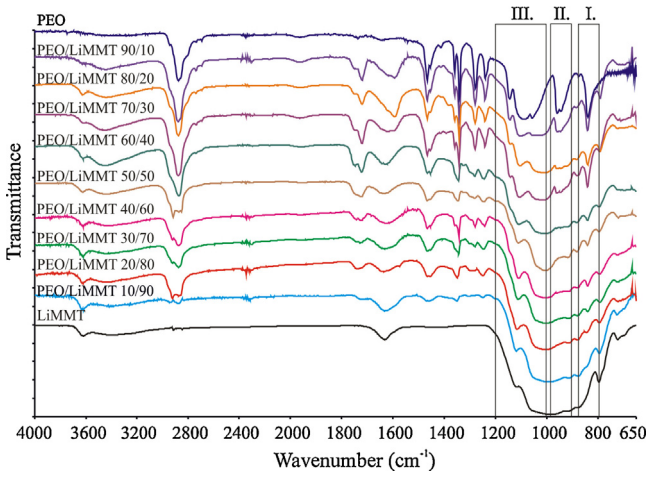


**Fig. 5.** Normalized FT-IR spectra of all analysed samples.

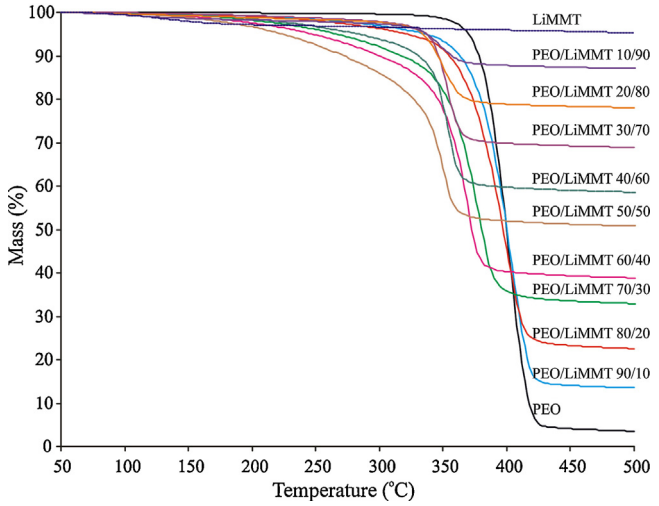


**Fig. 6.** TGA curves of all analysed samples.

are generally related to the $CH_2$ rocking vibrations in the gauche conformation required for the helical conformation of PEO [4,14]. These peaks can be observed in FT-IR spectra of pure PEO, indicating that pure PEO really is in helical conformation. The absence of the band at 1320 $cm^{-1}$ assigned to $CH_2$ vibrations in zigzag conformation also indicates helical conformation of PEO. As the amount of LiMMT increases the intensity of the peaks at 945 $cm^{-1}$ and at 840 $cm^{-1}$ decreases. The peak at 945 $cm^{-1}$ completely disappears above 40 wt.% of LiMMT while the peak at 840 $cm^{-1}$ can be observed up to 80 wt.% of LiMMT indicating that the helical structure of PEO in nanocomposites is highly distorted and above 80 wt.% of LiMMT it cannot be observed at all. The presence of three sharp peaks in the region of 1200–1000 $cm^{-1}$ (C–O–C stretching at 1144 $cm^{-1}$ and at 1090 $cm^{-1}$ and C–O stretching at 1058 $cm^{-1}$; designated with III. in Fig. 5) confirms the existence of a crystalline phase in pure PEO. In nanocomposites these peaks broaden and finally disappear at very high loadings of LiMMT, indicating the change of PEO crystallinity. Furthermore, the intensity of the bands that correspond to various methylene vibrations (1464 $cm^{-1}$ – assymetric methylene bending, 1358 $cm^{-1}$ – wagging, 1295 $cm^{-1}$ – twisting) are reduced due to the restricted space for polymer chains in the presence of LiMMT and due to the interactions of oxygen from PEO and $Li^+$ ions.

### 3.4. Non-isothermal thermogravimetry

The influence of LiMMT on the thermal stability of PEO is discussed only for the heating rate 10 °C/min since a similar behaviour is observed for all heating rates. Fig. 6 shows TGA curves of all samples. In the applied temperature region, LiMMT is thermally stable and the observed mass loss (approximately 5 wt.%) is attributed to its dehydratation and dehydroxylation. Thermal degradation of pure PEO and PEO/LiMMT nanocomposites occurs through one degradation step in the temperature range 190–450 °C, depending on the sample composition. In order to establish the influence of the LiMMT content on the thermal stability of PEO, the onset degradation temperatures ($T^o$) and the temperatures at the maximum degradation rate ($T_{max}$) were determined and given in Table 2.

PEO/LiMMT nanocomposites show lower $T^o$ and $T_{max}$ values compared to pure PEO. The $T^o$ values up to 50 wt.% LiMMT decrease almost linearly, while at higher LiMMT loadings the $T^o$ values show a slight increase and final decrease to a value similar to that of the PEO/LiMMT 50/50 sample.

A similar behaviour is observed for the $T_{max}$ values (except for the PEO/LiMMT 90/10 sample). $T^o$ and $T_{max}$ values for samples with more than 50 wt.% of LiMMT are 50–60 °C lower than for the

**Table 2**
Effect of the LiMMT content on the thermal characteristics of PEO.

| Value | PEO/LiMMT | | | | | | | | | |
|---|---|---|---|---|---|---|---|---|---|---|
| | 100/0 | 90/10 | 80/20 | 70/30 | 60/40 | 50/50 | 40/60 | 30/70 | 20/80 | 10/90 |
| $T^o$ (°C) | 378 | 374 | 366 | 346 | 341 | 318 | 332 | 336 | 328 | 318 |
| $T_{max}$ (°C) | 401 | 404 | 400 | 380 | 370 | 350 | 355 | 353 | 349 | 349 |
| $R_{max}$ (%/min) | 27.6 | 21.3 | 16.7 | 16.3 | 17.6 | 13.8 | 16.3 | 13.2 | 6.4 | 2.9 |
| $\alpha_{max}$ | 0.59 | 0.66 | 0.70 | 0.73 | 0.75 | 0.74 | 0.67 | 0.56 | 0.53 | 0.62 |
| $m_f$ (%) | 3.6 | 13.5 | 22.5 | 32.9 | 38.8 | 50.8 | 58.6 | 68.9 | 78.0 | 87.0 |

original PEO, respectively. Addition of LiMMT lowers significantly the thermal stability of PEO although it is generally believed that the introduction of inorganic components into organic materials improves their thermal stabilities due to the physical protective barrier and delayed volatization of degradation products [15]. A similar behaviour has been observed for some other polymer composites and nanocomposites. The residual mass, $m_f$ (Fig. 6, Table 2) increases linearly with the addition of LiMMT due to its thermal stability in this temperature range. The maximum degradation rate ($R_{max}$) of nanocomposites is lower compared to pure PEO (Table 2), while the conversion at the maximum degradation rate ($\alpha_{max}$) firstly increases up to 50 wt.% of LiMMT and then decreases. Changes in the $R_{max}$ and $\alpha_{max}$ values indicate possible changes in the mechanism of thermal degradation of PEO in the presence of LiMMT. In that sense, kinetic analysis can provide some useful information.

### 3.5. Kinetic analysis

Kinetic analysis, i.e. the determination of the activation energy of the non-isothermal degradation by the isoconversional Friedman (FR) [16] method is performed. Isoconversional methods are the most reliable methods for the calculation of the activation energy ($E$) and its dependence on the conversion, $\alpha$ [15,17]. Among isoconversional methods, the differential method of Friedman is the most universal one because it is applicable to a wide variety of temperature programs [15]. If $E$ is roughly constant over the whole conversion range and if no shoulders are observed in the reaction rate curve, it is likely that the process is dominated by a single reaction step [15]. Otherwise, the process is complex and the shape of the $E$ vs. $\alpha$ curve offers indications concerning the reaction mechanism [18]. FR method is based on Eq. (2):

$$\ln\left[\beta\frac{d\alpha}{dT}\right] = \ln A + \ln f(\alpha) - \frac{E_{FR}}{RT} \quad (2)$$

where $\beta$ is the linear heating rate, $R$ is the general gas constant, $T$ is the absolute temperature, $f(\alpha)$ is the kinetic model and $\alpha$ is the conversion defined as a fraction of the total mass loss in the process. It is calculated from the non-isothermal thermogravimetry experiment as the ratio $(m_0 - m)/(m_0 - m_f)$, where $m_0$, $m$ and $m_f$ are the initial, actual and residual mass of the analysed sample. For $\alpha$ = const., the plots $\ln[\beta d\alpha/dT)$ vs. $1/T$ obtained from $\alpha - T$ curves recorded at several heating rates should be straight lines whose slope allows the calculation of the activation energy, $E_{FR}$. An example is shown in Fig. 7.

PEO degradation occurs by the random-chain scission of C–O and C–C bonds [19,20]. Thermal degradation starts on the weak link sites inherent with the polymer chains which serve as spots where thermal degradation is initiated. The process of initiation at the weak links is characterized with low activation energy (up to conversion $\alpha$ = 0.06). Once the weak links have given way to initiation the effective activation energy increases. The nearly constant $E_{FR}$ values for pure PEO in the conversion range 0.06–0.96 (Fig. 8) suggest that the degradation kinetics is essentially limited by a single

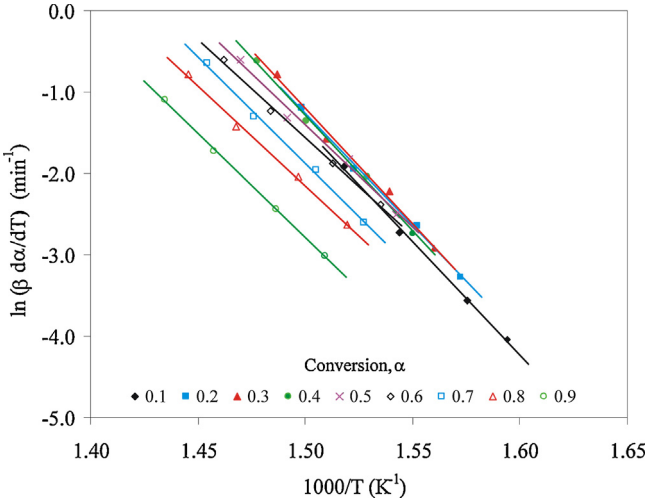


**Fig. 7.** Application of the FWO method on the PEO/LiMMT 80/20 sample.

reaction step, where the value of around 210 kJ mol$^{-1}$ corresponds to the above mentioned degradation mechanism.

All nanocomposites show different $E_{FR}$ values compared to pure PEO. Also, $E_{FR}$ vs. $\alpha$ dependency changes with the amount of LiMMT, except for sample with 10 wt.% of LiMMT which shows $E_{FR}$ vs. $\alpha$ dependency similar to pure PEO. Samples with 20–60 wt.% of LiMMT show initial increase of $E_{FR}$ in the broader conversion range compared to pure PEO and consequently plateau with constant $E_{FR}$ is achieved at higher conversions. Samples with more than 70 wt.% of LiMMT show additional increase of $E_{FR}$ at conversion higher than 0.80. Finally, the sample with 90 wt.% of LiMMT shows firstly a decrease of $E_{FR}$, then a sharp increase followed by a short

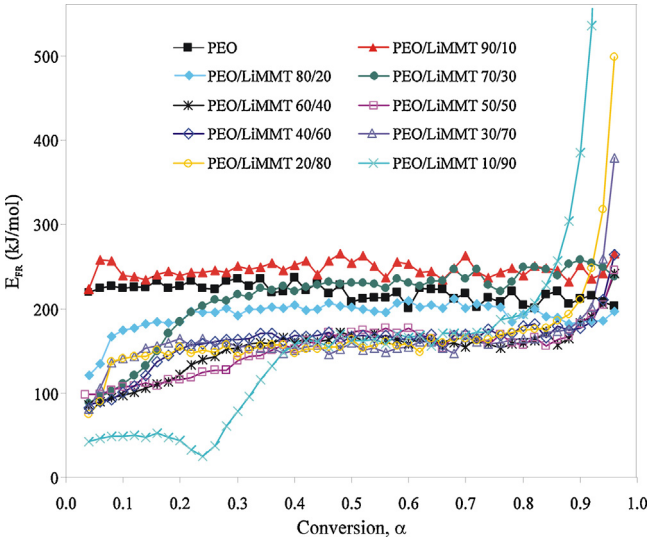


**Fig. 8.** The dependence of $E_{FWO}$ on $\alpha$ for pure PEO and PEO/LiMMT nanocomposites.

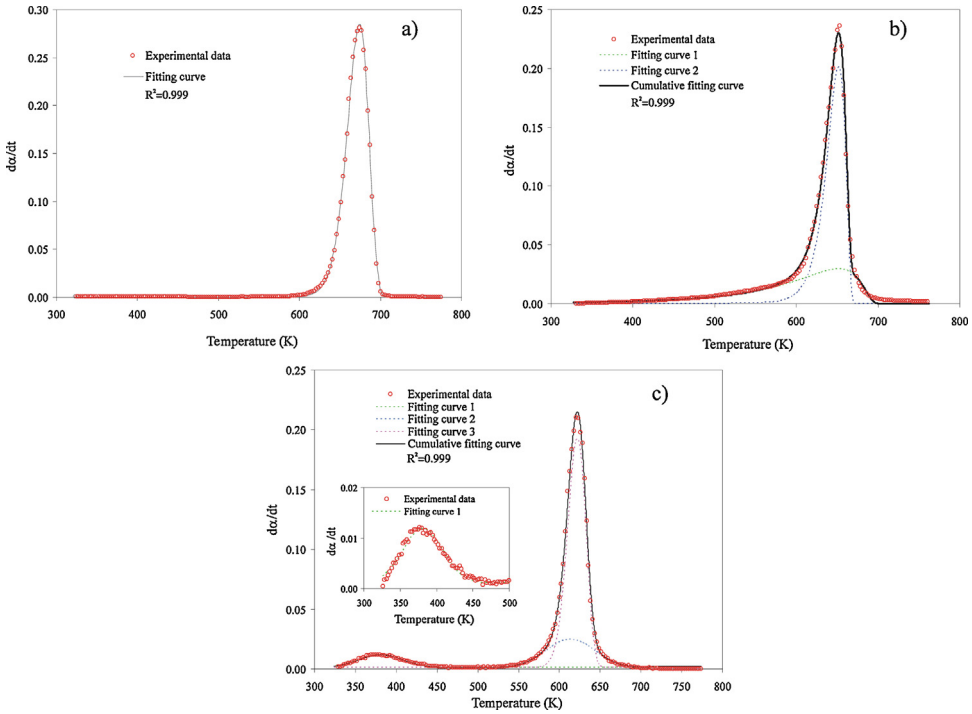


**Fig. 9.** Overlay of experimental kinetic curves at 10 °C/min (circles) and fitted (dotted) and cumulative (solid lines) kinetic curves for pure PEO (a), PEO/LiMMT 70/30 (b) and PEO/LiMMT 10/90 (c).

plateau and a final increase of $E_{FR}$. These results, as explained above, indicate that LiMMT influences, i.e. makes the mechanism of the PEO thermal degradation more complex. To justify this statement, a deconvolution procedure described in details by Perejón et al. [21] and Sánchez-Jiménez et al. [22] has been performed. Origin 9 computer program and different fitting functions (Gaussian, Lorentzian and Frazer-Suzuki) have been used for the deconvolution process.The fitting results for the three selected samples (PEO, PEO/LiMMT 70/30 and PEO/LiMMT 10/90) are given in Fig. 9.

Fig. 9 shows experimental thermogravimetric curves (circles) in their differential form ($d\alpha/dt$) at 10 °C/min, fitted (dotted) and cumulative (solid lines) kinetic curves. Cumulative curves are obtained by summation of individual fitting curves. It is obvious from Fig. 9a that pure PEO kinetic curve is symmetrical and can be well fitted (correlation coefficient, $R^2 = 0.999$) with only one Gaussian function, supporting the above mentioned conclusion that its thermal degradation is essentially limited by a single reaction step. Fig. 9b clearly shows that kinetic curve of PEO/LiMMT 70/30 is asymmetrical and can be well fitted with two Frazer–Suzuki functions whose cumulative curve fits experimental one with $R^2 = 0.999$. This practically means that thermal degradation of PEO/LiMMT 70/30 can be described by two independent processes that take place simultaneously. Similar results are obtained for other PEO/LiMMT samples except PEO/LiMMT 10/90. Namely, its thermal degradation can be described by three independent processes ($R^2 = 0.999$) as shown in Fig. 9c. These results support earlier indications obtained by Friedman method that LiMMT really makes thermal degradation of PEO more complex.

### 3.6. Conductivity

The conductivity is measured by sandwiching PEO/LiMMT nanocomposites between the stainless steel electrodes. Representative impedance spectroscopy plot for PEO/LiMMT nanocomposite containing 40 wt.% of LiMMT is shown in Fig. 10.

From these plots conductivity values ($\sigma$) were calculated by measuring the bulk resistance ($R_b$) of the electrolyte. $R_b$ is derived as the touch point at zero imaginary part value (Fig. 10). The conductivity values ($\sigma$) are calculated according to the Eq. (3):

$$\sigma = \frac{t}{R_b A} \tag{3}$$

where $t$ is thickness and $A$ area of PEO/LiMMT nanocomposites.

Fig. 11 displays the calculated ionic conductivity for PEO/LiMMT nanocomposites at room temperature.

Conductivity increases with an increase in LiMMT content and attains a maximum value of $2.8 \times 10^{-6}$ S/cm when the LiMMT concentration is 40 wt.% what is 949 times higher than conductivity of pure PEO ($2.9 \times 10^{-9}$ S/cm). Subsequently, the ionic conductivity decreases with further increases in LiMMT content up to 80 wt.% but always remains higher than one for pure PEO. It is generally accepted that addition of inorganic fillers can increase conductivity of SPEs in two ways [23]: (1) by increasing the ratios of the ammorphous phase (reducing the crystallinity degree) of PEO matrix and (2) providing $Li^+$ conducting pathways at the surface regions of the fillers through Lewis acid–base interactions. Our conductivity measurements were performed at 25 °C, i.e. below melting temperataure of PEO. In this case, influence on conductivity is mainly

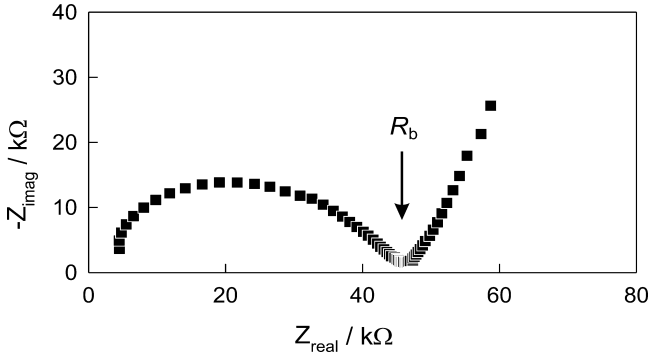


**Fig. 10.** Impedance spectroscopy plot for PEO/LiMMT 60/40 nanocomposite.

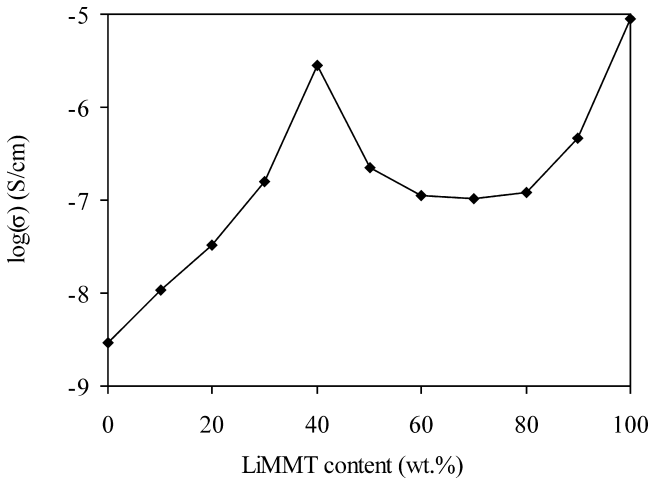


**Fig. 11.** Room temperature ionic conductivity of PEO/LiMMT nanocomposites.

attributed to the lower the crystallinity of PEO with the addition of LiMMT. Our results show that addition of LiMMT leads to a higher ionic conductivity by reducing the PEO crystallinity as observed from the DSC results [23]. But, once the optimum LiMMT content is crossed, the ionic conductivity falls. Obviously, the degree of crystallinity is not the only factor that influences ionic conductivity since the changes of conductivity are not in accordance with changes in crystallinity in the whole composition range. This means that dispersion of LiMMT also influences ionic conductivity in this system. At lower contents, LiMMT is well-dispersed allowing favourable environment for $Li^+$ ion mobility. Amount of LiMMT over 40 wt.% leads to self-aggregation between the silicate layers which tightly hold $Li^+$ ions and reduces their mobility and consequently reduces conductivity of PEO/LiMMT nanocomposites. These results are compared with the earlier studies of the conductivity of PEO nanocomposites with lithium modified clays. Manoratne et al. [3] have measured the ionic conductivity of PEO/LiMMT nanocomposites of $3.03 \times 10^{-8}$ S/cm at room temperature. Moreno et al. [24] have measured the ionic conductivity of PEO/bentonite-Li+ nanocomposites of $3.89 \times 10^{-8}$ S/cm and $1.79 \times 10^{-8}$ S/cm where PEO molecular weight is 600,000 and 40,000,000, respectively. In this sense, the results obtained in this work are improved for two orders of magnitude.

## 4. Conclusions

PEO/LiMMT nanocomposites with 10–90 wt.% of LiMMT were prepared by the melt intercalation method. According to SAXS analysis, the gallery spacing of LiMMT in PEO/LiMMT samples is expanded due to the intercalation of the PEO chain, i.e. to the formation of a nanocomposite structure. SAXS also shows that LiMMT has an ability to reduce the crystalline nature of PEO. The crystallinity of PEO continuously decreases with addition of LiMMT and above 80 wt.% of LiMMT it cannot be observed at all. The PEO melting temperature also decreases with addition of LiMMT, and the highest decrease is observed for the sample with 50 wt.% of LiMMT. FT-IR analysis also proofs that a more pronounced change in the conformation and crystallinity of PEO occurs at higher LiMMT loadings and that above 80 wt.% of LiMMT the helical structure of PEO cannot be observed at all. The thermal stability of PEO is lower in nanocomposites where the lowest thermal stability is observed for the sample with 50 wt.% of LiMMT. LiMMT influences the thermal degradation mechanism of PEO, as indicated by changes of the maximum degradation temperature, conversion at the maximum degradation rate and kinetic analysis. All PEO/LiMMT nanocomposites show higher ionic conductivity compared to pure PEO. It is established that addition of 40 wt.% of LiMMT is optimum in terms of ionic conductivity since it is increased for 949 times compared to ionic conductivity of pure PEO.

## Acknowledgement

This work is financially supported by the Ministry of Science, Education and Sports of the Republic of Croatia (scientific project “Polymer blends with biodegradable components”).

## References

[1] G. Sandí, K.A. Carrado, H. Joachin, W. Lu, J. Prakash, Polymer nanocomposites for lithium battery applications, J. Power Sources 119–121 (2003) 492–496.
[2] E. Quartatone, P. Mustarelli, A. Magistris, PEO-based composite polymer electrolytes, Solid State Ion. 110 (1998) 1–14.
[3] C.H. Manoratne, R.M.G. Rajapakse, M.A.K.L. Dissanayake, Ionic conductivity of poly(ethylene oxide) (PEO)-montmorillonite nanocomposites prepared by intercalation from aqueous medium, Int. J. Electrochem. Sci. 1 (2006) 32–46.
[4] Z. Shen, G.P. Simon, Y. Cheng, Saturation ratio of poly(ethylene oxide) to silicate in melt intercalated nanocomposites, Eur. Polym. J. 39 (2003) 1917–1924.
[5] W. Loyens, P. Jannasch, F.H.J. Maurer, Effect of clay modifier and matrix molar mass on the structure and properties of poly(ethylene oxide)/Cloisite nanocomposites via melt-compounding, Polymer 46 (2005) 903–904.
[6] H.J. Choi, S.G. Kim, Y.H. Hyun, M.S. Jhon, Preparation and rheological characteristics of solvent-cast poly(ethylene oxide)/montmorillonite nanocomposites, Macromol. Rapid Commun. 22 (2001) 320–325.
[7] H.-W. Chen, F.-C. Chang, The novel polymer electrolyte nanocomposite composed of poly(ethylene oxide), lithium triflate and mineral clay, Polymer 42 (2001) 9763–9769.
[8] C.-S. Liao, W.-B. Ye, Enhanced ionic conductivity in poly(ethylene oxide)/layered double hydroxide nanocomposites electrolytes, J. Polym. Res. 10 (2003) 241–246.
[9] D. Ratna, S. Divekar, A.B. Samui, B.C. Chakraborty, A.K. Banthia, Poly(ethylene oxide)/clay nanocomposite: thermomechanical properties and morphology, Polymer 47 (2006) 4068–4074.
[10] F. Croce, G.B. Appetecchi, L. Persi, B. Scrosati, Nanocomposite polymer electrolytes for lithium batteries, Nature 394 (1998) 456–458.
[11] T.J. Benedict, S. Banumathi, A. Veluchamy, R. Gangadharan, A.A. Zulfihar, S. Rajendran, Characterization of plasticized solid polymer electrolyte by XRD and AC impedance methods, J. Power Sources 75 (1998) 171–174.
[12] K.E. Strawhecker, E. Manias, Crystallization behavior of poly(ethylene oxide) in the presence of $Na^+$ montmorillonite fillers, Chem. Mater. 15 (2003) 844–849.
[13] S. Zheng, K. Nie, Q. Guo, Miscibility and phase separation in blends of phenolphtalein poly(aryl ether ketone) and poly(ethylene oxide): a differential scanning calorimetry study, Thermochim. Acta 419 (2004) 267–274.
[14] Y. Gnanou, M. Fontanille, Organic and Physical Chemistry of Polymers, John Wiley&Sons Inc, New Jersey, 2008, pp. 554.
[15] S. Vyazovkin, A.K. Burnham, J.M. Criado, L.A. Pérez-Maqueda, C. Popescu, N. Sbirrazzuoli, ICTAC Kinetis Committee recommendations for performing kinetic computations on thermal anaylsis data, Thermochim. Acta 520 (2011) 1–19.
[16] H.L. Friedman, Kinetics of thermal degradation of char-foaming plastics from thermogravimetry application to a phenolic resin, J. Polym. Sci. 6C (1963) 183–195.
[17] S. Vyazovkin, N. Sbirrazzuoli, Isoconversional kinetic analysis of thermally stimulated processes in polymers, Macromol. Rapid Commun. 27 (2006) 1515–1532.
[18] P. Budrugeac, E. Segal, L.A. Pérez-Maqueda, J.M. Criado, The use of the IKP method for evaluating the kinetic parameters and the conversion function of the thermal dehydrochlorination of PVC from non-isothermal data, Polym. Degrad. Stab. 84 (2004) 311–320.
[19] P. Sainte Claire, Degradation of PEO in the solid state: a theoretical kinetic model, Macromolecules 42 (2009) 3469–3482.
[20] K. Pielichowski, K. Flejtuch, Non-oxidative thermal degradation of poly(ethylene oxide): kinetic and thermoanalytical study, J. Anal. Appl. Pyrol. 73 (2005) 131–138.
[21] A. Perejón, P.E. Sánchez-Jiménez, J.M. Criado, L.A. Pérez-Maqueda, Kinetic analysis of complex solid-state reactions. a new deconvolution procedure, J. Phys. Chem. B 115 (2011) 1780–1791.
[22] P.E. Sánchez-Jiménez, L.A. Pérez-Maqueda, A. Perejón, J.M. Criado, Nanoclay nucleation effect in the thermal stabilization of a polymer nanocomposite: a kinetic mechanism change, J. Phys. Chem. C 116 (2012) 11797–11807.
[23] J. Xi, X. Qiu, X. Ma, M. Cui, J. Yang, X. Tang, W. Zhu, L. Chen, Composite polymer electrolyte doped with mesoporous silica SBA-15 for lithium polymer battery, Solid State Ionics 176 (2005) 1249–1260.
[24] M. Moreno, R. Quijada, M.A. Santa Ana, E. Benavente, P. Gomez-Romero, G. González, Electrical and mechanical properties of poly(ethylene oxide)/intercalated clay polymer electrolyte, Electrochim. Acta 58 (2011) 112–118.